Handwritten, Soft Circuit Boards and Antennas Using Liquid Metal Nanoparticles

Yiliang Lin, Christopher Cooper, Meng Wang, Jacob J. Adams, Jan Genzer, and Michael D. Dickey**

This paper describes a simple method to fabricate soft circuit boards, antennas, and conductive paths composed of liquid metal nanoparticles embedded in an elastomeric matrix. These films of nanoparticles become electrically conductive after applying localized pressure that merges the particles together to form conductive traces. Two concepts motivate this work: (1) The ability to create an analog of circuit boards out of soft materials, which offers a route to connect circuit elements for unconventional electronics and (2) the ability to "draw" antennas to a desired geometry on demand, which is appealing for customizing communication devices on the fly.

Soft, flexible, and stretchable electronics have attracted immense attention recently because of the unique applications enabled by these mechanical properties.[1–3] Taking advantage of thin form factors,[4] flexible devices have been fabricated using rigid materials with limited stretchability and deformability.[2,5] The use of intrinsically soft materials removes this limitation, albeit often at the expense of electronic performance.[6] Soft materials with good electronic performance are desired and fluidic conductors, such as liquid metals and conductive pastes, represent such class of materials.[7–9] These fluids are soft and maintain metallic conductivity even at large deformations due to the ability to distort with the encapsulating material.[10,11]

Here, we utilize eutectic gallium indium (EGaIn) due to its low melting point (m.p. ≈ 15.5 °C).[8,12] Because of its low toxicity[13] and high conductivity ($\sigma = 3.4 \times 10^4\,\mathrm{S\,cm^{-1}}$[14], EGaIn may be applied to microfluidic systems and soft electronics, such as memristors,[6] stretchable wires,[10,11] antennas,[15–17] sensors,[18,19] capacitors,[20] and reconfigurable circuits.[21] The ability to induce the metal to flow by applying external pressure offers a route for changing the shape and, in some cases, the conductivity of circuit elements on demand. Here, we embed films of EGaIn nanoparticles in elastomer matrix and "sinter" them selectively using localized pressure to form locally conductive pathways.

Most films and patterned traces of metallic particles have limited (or no) conductivity. Sintering merges the particles into conductive paths. Various sintering methods exist, such as thermal sintering,[22] photonic sintering,[23] light sintering,[24–26] or laser sintering.[27] Thermal sintering requires a significant input of energy over an extended time period while exposing the underlying substrate to elevated temperatures. Photonic sintering, flash sintering, and laser sintering all require specialized equipment and usually expose the underlying substrate to short thermal excursions. The use of particles composed of liquids enable "mechanical sintering"—a concept introduced by the Kramer group[28]—in which the particles merge together in response to pressure in a manner analogous to rupturing miniature water balloons. Mechanical sintering can be done at room temperature, which makes it compatible with a wide range of materials. It can also be performed without utilizing specialized equipment.

Mechanical sintering has been employed to form conductive traces in exposed films of the metal[28] and in particles distributed in elastomer.[29] Here, we demonstrate that it is possible to embed films of such EGaIn particles to create soft circuit boards. We also show it is possible to inject and then sinter these particles in microchannels to form conductive pathways that can serve as antennas with tunable frequencies. Mechanical sintering allows these soft circuit boards and antennas to be designed arbitrarily by hand simply with a writing utensil. There are a number of ways to create conductive elastomers including embedding conductive particles (e.g., carbon nanotubes[30,31] or steel wool[32]). Here, the elastomers are only rendered locally conductive after applying pressure at specific locations. In addition, by localizing the particles to thin films, the resulting traces are an order of magnitude more conductive than when they are dispersed in the elastomer.[29] The improved conductivity enables the manufacture of antennas and circuit boards on demand. In addition, we show that it is possible to form high-resolution patterns of liquid metal particles either by laser sintering films of particles or by injecting them into microfluidic devices. To demonstrate the utility, we fabricate antennas with tunable operating wavelengths by applying localized pressure, which provides a new way for "drawing" antennas by hand with frequencies determined on demand.

While particles of liquid metal could be obtained by molding[33] or flow focusing,[34,35] we utilized sonication[36]

Y. Lin, C. Cooper, Prof. J. Genzer, Prof. M. D. Dickey
Department of Chemical and Biomolecular Engineering
North Carolina State University
Raleigh, NC 27695-7905, USA
E-mail: jgenzer@ncsu.edu; mddickey@ncsu.edu
M. Wang, Prof. J. J. Adams
Department of Electrical and Computer Engineering
North Carolina State University
Raleigh, NC 27695-7911, USA

DOI: 10.1002/smll.201502692

www.MaterialsViews.com

due to its simplicity and ability to form nanoscale droplets. To synthesize EGaIn NPs, 2 g EGaIn was added into a 20 mL vial filled with 10 mL of ethanol, as shown in **Figure 1**a. Probe sonication produced a gray suspension, as shown in Figure 1b. It took only 10 min to create the suspension; this is much faster compared to bath sonication.[36] Although larger particles settle to the bottom of the vial, nanoparticles produced in ethanol remained suspended up to several weeks, while those formed in water, benzene, and dodecane precipitated within tens of minutes (see Figure S1, Supporting Information). Figure 1c shows a representative transmission electron microscopy (TEM) image of particles taken from the suspension. The particle size distribution was determined from examining dimensions of ≈180 particles by scanning electron microscopy (SEM). The average diameter of the EGaIn NPs is ≈105 nm and a Gaussian distribution fits the variation well. The energy provided by probe sonication fractures the oxide coating and breaks EGaIn drops into smaller particles, which form a fresh skin of oxide. A high resolution TEM of these nanoparticles reveals two concentric layers of coating on the particle. The inner shell (gallium oxide) is ≈3 nm thick, as seen in Figure 1d. Imaging with a Titan scanning transmission electron microscope (STEM) (Figure 1e**)** provided element mapping on EGaIn NPs (Figure 1f). As expected, indium and gallium appear in the core of the particle, while oxygen and gallium are present in the shell. In addition, there is carbon present on the outer surface of the particles. These results indicate that (1) the oxide comprises gallium oxide instead of indium oxide, as expected,[8,37] (2) a carbon coating surrounds the gallium oxide, (3) the thickness of the gallium oxide layer is ≈3 nm, and (4) the observation of a carbon layer is consistent with the high resolution TEM image (Figure 1d). While it is possible that the carbon detected in the sample constitutes adventitious carbon, we did not detect the carbon layer when using dodecane instead of ethanol. We suspect that the carbon layer outside the gallium oxide may act as a surfactant with the ethanol solvent, which may explain the stability of EGaIn suspension over many hours in ethanol but not in water.

Figure 2a depicts the process for fabricating a soft circuit board. Typically, we start with a sheet of poly(dimethylsiloxane) (PDMS) elastomer (commercial kit Sylgard-184, obtained from Dow Corning). We chose PDMS elastomer because it is used commonly for soft electronics due to its low modulus (≈2 MPa) and ease of processing. The PDMS elastomer supports a film composed of EGaIn particles formed by casting the suspension of EGaIn NPs on top of the PDMS. Slight shaking and tilting the PDMS after casting the EGaIn layer facilitates a uniform coating. Slowing the ethanol evaporation rate helps minimize cracking in the film. For example, drying the samples at 0 °C reduces the density of defects relative to the samples dried at ambient conditions. After solvent evaporation, we spread a PDMS prepolymer on the EGaIn films and cure it thermally to form a sandwich-like structure.

The film of EGaIn NPs forms an insulating film due to the oxide coating on the particles, but the particles merge in response to external pressure applied locally to the PDMS elastomer overcoat to form conductive paths. To demonstrate the concept, we use a marker to generate the mechanical pressure and visualize the location of the applied pressure. Figure 2b shows that the initially nonconductive film between the two electrical leads becomes electrically conductive upon application of mechanical pressure using a marker. Video S1 (Supporting Information) shows the process of creating a simple circuit board with a light emitting diode (LED). We measured the *I–V* curve before and after mechanical sintering (Figure S2, Supporting Information). Even at 30 V, the current is only 1.85×10^{-8} A (corresponding to a resistance of $1 \times 1\ 0^{9}$ Ω between two electrodes placed ≈4 mm apart

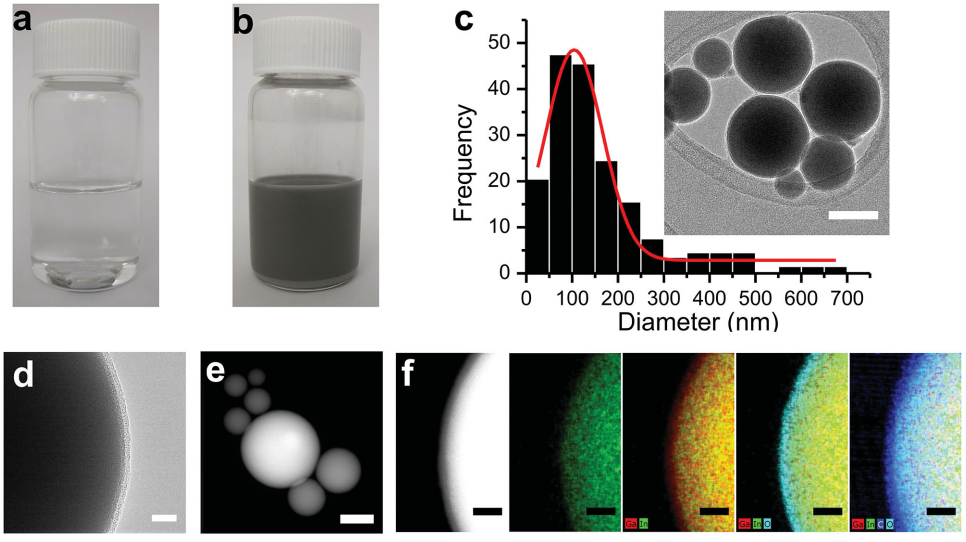

Figure 1. Characterization of EGaIn nanoparticles. a) EGaIn in ethanol solvent before probe sonication. b) EGaIn suspension after probe sonication. c) Size distribution of EGaIn particles. Mean diameter is ≈105 nm and is fit by a Gaussian distribution. Thumbnail is a typical TEM image of EGaIn NPs under JEOL 2010F. The scale bar is 50 nm. d) A TEM image for EGaIn coating. The black core is the liquid metal and the lighter part is the coating. Two layers of coating could be observed; the inner coating (gallium oxide) is ≈3 nm thick. The scale bar is 5 nm. e) A typical STEM image of EGaIn NPs. The scale bar is 50 nm. f) Element mapping of the EGaIn coating. From left to right, the picture shows EGaIn NPs; In (green); Ga (red), and In (green); Ga (red), In (green), and O (cyan); Ga (red), In (green), O (blue), and C (cyan). The scale bar is 10 nm.

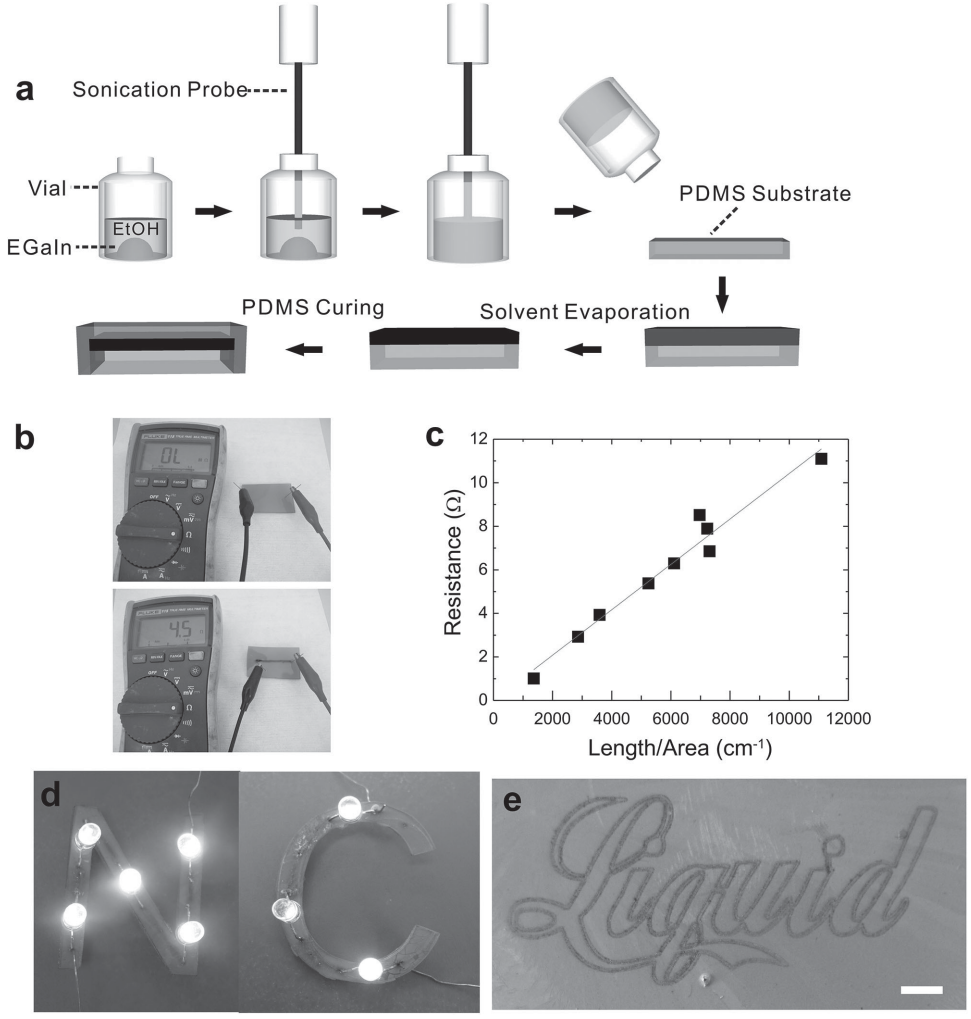

Figure 2. Fabrication and characterization of a soft circuit board. a) Schematic design of the soft circuit board. b) A rectangle circuit board inserted with two copper wires. The path between the copper wires is initially nonconductive. After applying external pressure using a marker, the path becomes conductive with a resistance of 4.5 Ω. c) Linear plot for the resistivity data of the soft circuit board. The slope (resistivity) is 0.00104 Ω cm; the fit quality is $R^2 = 0.96$. d) A "NC" soft circuit board with LEDs. e) A laser sintered sample with a conductive "Liquid" pattern. The scale bar is 3 mm.

and a film ≈1 mm wide and ≈15 μm thick). In contrast, after sintering, the conductivity increases by a factor of 4×10^8. Figure 2c plots the resistivity as a function of trace length measured by a four-point probe method. The slope (resistivity) is $0.0010 \Omega\text{cm}$, thus the conductivity is $9.6 \times 10^2\ \text{Scm}^{-1}$, which is almost ten times that of liquid metal particles distributed and sintered in PDMS elastomer while using ≈30 times less metal than composites with the same overall weight. Composites of PDMS–Galinstan (typically 68 wt% Ga, 22 wt% In, and 10 wt% Sn) have a different application space and are mentioned here only for comparison.[29]

Conventional printed circuit boards (PCBs) require multiple process steps to fabricate functional devices, i.e., copper patterning and subtractive, additive, and semiadditive processes. The copper traces in the PCB must be designed in advance of use and the PCBs are not soft. Figure 2 shows that it is possible to fabricate a soft circuit board on demand, albeit using much simpler geometries with lower resolution. The resulting circuit boards can be cut into a desired shape during an optional postprocessing step. Figure 2d shows circuit boards fabricated with LEDs. It is possible to connect rigid components into soft interconnects by simply inserting them into the PDMS elastomer in a manner that is analogous to a bread board. Electrical components (e.g., LEDs) can be readily inserted into the circuit boards without soldering. The circuit boards could be flexed and stretched without delamination. Placing the samples in acid, which removes the surface oxide layer, does not cause the samples to delaminate. This suggests that a sufficient amount of polymer spans the top and bottom pieces of PDMS elastomer to ensure adhesion. A drawback of this approach is that particles may sinter inadvertently if exposed to excessive pressures, which makes it difficult to ensure insulating regions remain insulating. In a preliminary experiment, we found that curing a rigid layer of polymer (Norland Optical Adhesive) on the surface of PDMS helps distribute inadvertent stress, which could potentially prevent undesired sintering after a circuit is "written." A more elegant long-term solution may be to use embedding materials that can be stiffened after sintering (e.g., polyvinylmethylsiloxane[38]).

Another limitation of this approach for forming interconnects is the relatively low resolution of the traces. The use of

www.MaterialsViews.com

a stylus to generate localized mechanical pressure through the PDMS elastomer limits the resolution to several millimeters. Although mechanical sintering can form traces as small as 20 μm in exposed films,[28] the PDMS elastomer sheet that embeds the particles distributes the pressure and widens the effective trace. We found that laser sintering of the films of particles could form conductive patterns by exposing the particle films to a desktop laser (Universal Laser System VLS 3.50). Figure 2e shows a laser sintered sample with a conductive trace of the word "Liquid" patterned on it. These traces have higher resolution than those produced by hand but require specialized equipment and are therefore only shown to demonstrate that traditional sintering methods also work.

One simple approach to increase the resolution is to inject the particles into microfluidic channels. Injecting the metal into microchannels requires pressure since the liquid metal has a large surface tension and an oxide skin. In contrast, dispersing the particles in solvent creates a suspension with fluid properties dominated by the solvent, which makes it easier to inject the metal into microchannels relative to the pure metal. Filling a microchannel with a cross-sectional area of 50×300 μm^2, it requires 45 kPa to inject pure EGaIn but only 15 kPa to deliver EGaIn–ethanol suspension. In addition, it is possible to create nonconductive traces that may be rendered conductive via pressure. **Figure 3**a illustrates the procedure to fabricate the microfluidic devices, which begins by standard soft replica molding.[39] It is straightforward to inject a suspension of EGaIn NPs (1 g mL^{-1} in ethanol) into the microchannels. Once inside the channels, the ethanol evaporates naturally due to the gas permeability of PDMS.[40,41] Although the channels are insulating after injection of the metallic particles, it is possible to mechanically sinter the particles in the microchannels. Figure 3b shows a microfluidic device patterned with the NC State logo.

We reason that under mechanical pressure, the gallium oxide that separates the NPs breaks and the metal merges together, forming a conductive path. SEM imaging provides morphological insight of EGaIn NPs in microchannels before and after mechanical sintering. Figure 3c,d depicts SEM images before mechanical sintering and EGaIn particles could be observed. A smooth morphology appears after mechanical sintering (Figure 3e,f). Particles merge when the "ceiling" of the microchannel presses against the film of NPs with sufficient force (in the absence of force, there is a gap between the film of particles and the "ceiling" of the channel). Thicker PDMS layers should distribute the applied pressure more than thin layers. To test this hypothesis, we measured the pressure needed to sinter particles in a PDMS microchannel as a function of the thickness of the PDMS overlayer. After sealing a PDMS microchannel on a glass slide patterned with gold electrodes, we pressed the PDMS with a 2 mm wide sheet of acrylic centered above the channel (1 mm wide and 50 μm deep) and recorded the pressure necessary to create a conductive pathway between the electrodes (Figure 3g). The pressure required for sintering increases with the thickness of the PDMS (Figure 3h). In previous work, Boley et al.[28] investigated the activation force per particle for EGaIn NPs of various diameters. Based on those findings, the necessary sintering pressure for EGaIn NPs with 100 nm

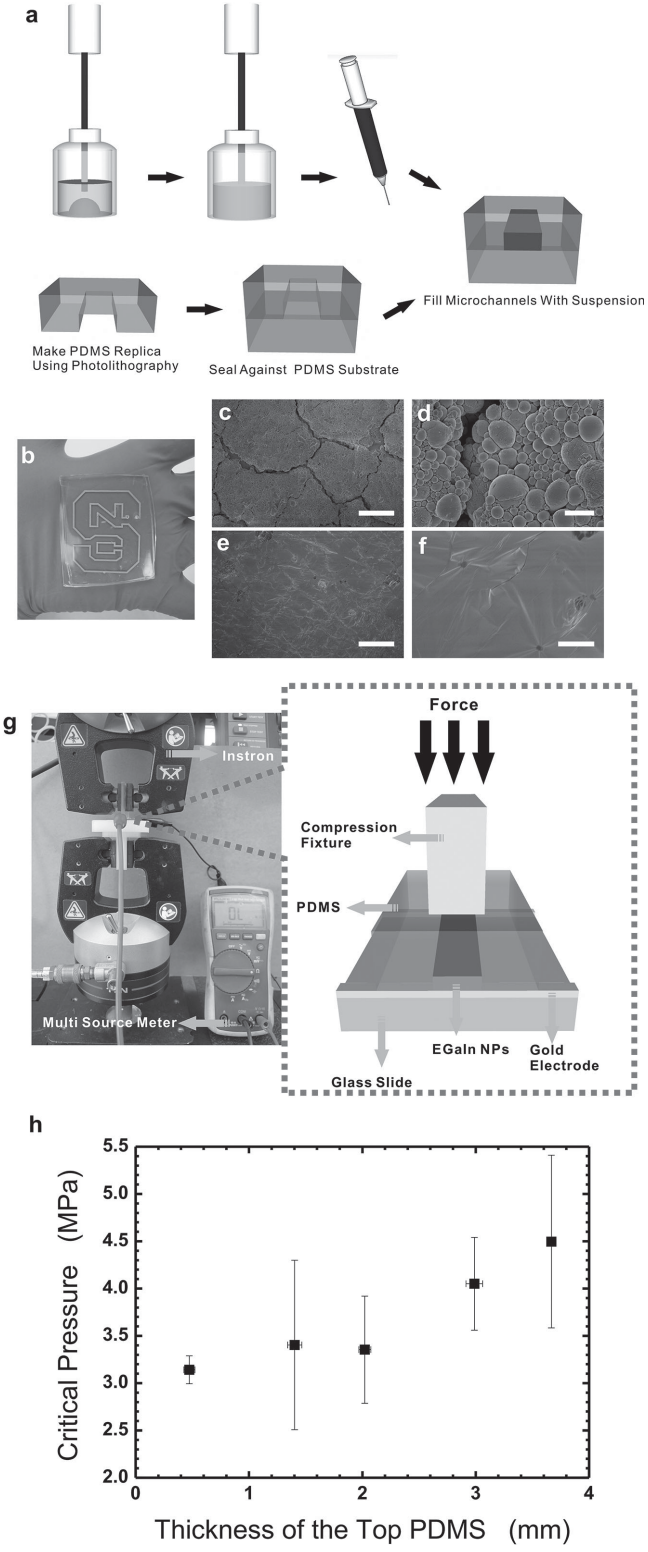

Figure 3. Fabrication and characterization of microfluidic devices that can be sintered mechanically. a) Schematic design of the microfluidic devices. b) A microfluidic device with "NCSU" logo. c,d) SEM images of liquid metal particles in the channel before sintering. The scale bars are 25 and 10 μm, respectively. e,f) SEM images of the particles after sintering. The scale bars are 25 and 10 μm, respectively. g) Experimental design of sintering pressure measurement. h) Plot of the sintering pressure versus thickness of the PDMS overlayer.

diameter would be ≈10 MPa, which is much larger than the pressure measured here. However, Figure 3d indicates that the presintered NPs have diameters >1 μm, which requires <1 MPa for sintering. SEM images suggest the ≈100 nm particles merge into larger particles as the ethanol-particle mixture becomes more concentrated. Considering the presence of the larger particles, we interpret the pressures reported in Figure 3g as those necessary to deform the PDMS.

To demonstrate the utility of these microfluidic devices in a wireless communication context, we fabricated an antenna with an operating frequency that can be tuned by mechanically sintering particles in a microchannel. Liquid metal antennas have been fabricated in PDMS previously by injection.[15–17] However, the antennas here can be drawn on demand as demonstrated below. Because antennas are typically narrowband, their frequency response must be customized for different applications and our approach offers a simple way to generate differing frequency responses on demand. To demonstrate the concept, we create a dipole antenna, which has an operating frequency that is inversely proportional to the conductor length. We injected an EGaIn suspension into two microchannels (25 mm long, 1 mm wide, and 50 μm thick channels) aligned along their long axis and separated by a 2 mm gap. **Figure 4**a,b shows the antenna and its flexibility. Before mechanical sintering, the traces of particles are electrically insulating and do not radiate as an antenna. We used mechanical sintering to elongate conductive traces that form the antenna and thereby tune the frequency. Figure 4c shows a schematic design for four antenna states as the conductive length varies from 0 to 25 mm. We measured the reflection coefficient of the antennas using a radio frequency network analyzer (Agilent E5071C) and recorded the responses for different states (lengths) of the antenna. A low reflection coefficient indicates that the antenna matches the source impedance and radiates the incident energy. Reflection coefficient values below –10 dB are generally considered effective. As shown in Figure 4d, the antenna does not radiate (reflection coefficient near 0 dB) until the pressure activates the antenna. Upon activation, the resonant frequency shifted from 3 to 1.8 GHz as the conductive length changed from 15 to 25 mm. The resonant frequencies agree well with simple dipole theory based on the lengths of the antennas and permittivity of the PDMS substrate. In principle, any resonant frequency between 1.8 and 3 GHz could be achieved by mechanically sintering the appropriate length using the geometries shown here. This sintering technique may be useful for rapid prototyping of antennas without the need for machining or for creating customized antennas in remote locations.

In conclusion, we developed a facile method to create soft circuit boards and tunable antennas by mechanically sintering films and microfluidic traces of EGaIn nanoparticles. Films of EGaIn particles cast in PDMS remain insulating until mechanical sintering merges them together to form conductive traces. In addition, it is possible to use intense light to irradiate the particles for higher resolution sintering, yet more complex, fabrication. The resolution of the traces can be improved by injecting the particles into microchannels. The thickness and the substrate of the microfluidic devices could be tuned to change the critical pressure of mechanical sintering. An antenna drawn by hand to arbitrary frequencies demonstrates the benefit of mechanical sintering.

PDMS comprises the antennas fabricated here, but the principles could extend to other encasing materials with

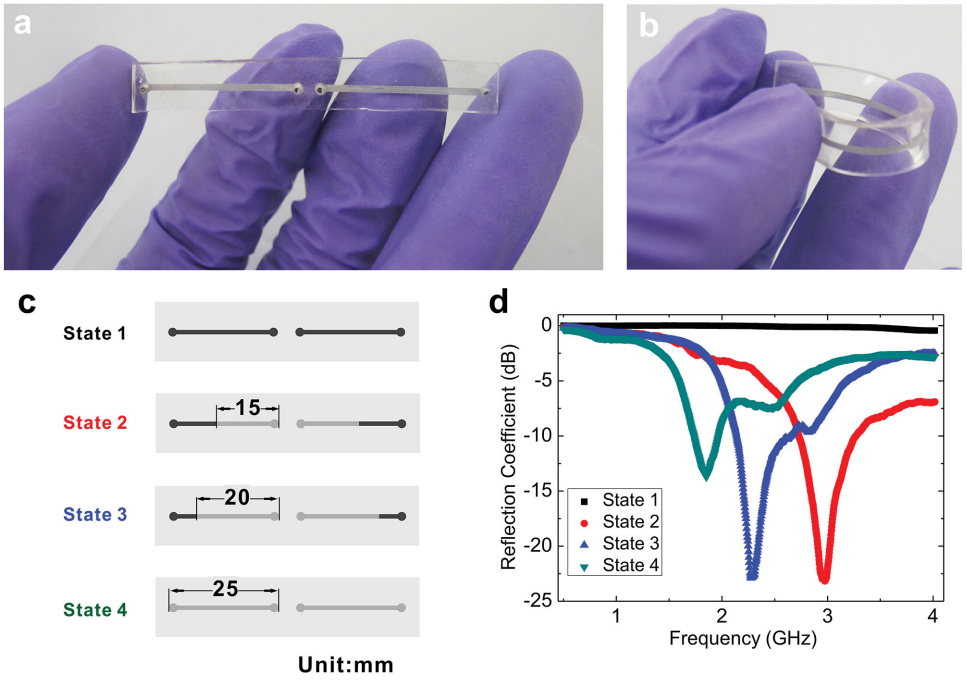

Figure 4. Fabrication and characterization of a tunable dipole antenna formed on demand by mechanical sintering. a,b) Flexible antenna injected with a suspension of EGaIn particles. c) Schematic design of the antenna with different conductive lengths tuned by mechanical pressure. d) Measured reflection coefficient of an antenna with different conductive lengths. With the increased conductive lengths from 15 to 25 mm, the resonant frequency shifts from 3 to 1.8 GHz.

a range of chemical and mechanical compositions. Future research could investigate other practical aspects of these soft conductors such as determining the resolution limit, exploring electrical and mechanical reliability, elucidating the role of nonsintered particles on performance, and extending this concept to more complex antenna systems. Creating films without cracks is another opportunity for future optimization.

Experimental Section

EGaIn Suspension Preparation and Characterization: To form a suspension of EGaIn, 2 g of EGaIn was added into a vial (20 mL), which was filled with ethanol to a total volume of 10 mL. A Q55 Sonicator (QSONICA) was used for sonication. The amplitude of the sonicator was adjusted to 80 and the sonication proceeded for 10 min. The suspension was cast onto a cured PDMS slab (Sylgard-184, Dow Corning). For suspension injected into microchannels, the suspension was concentrated to 2 g/2 mL (EGaIn/ethanol) after evaporating some ethanol. For SEM characterization (Figure 1), the suspension was diluted with ethanol by a factor of 50 and deposited dropwise on a clean silicon wafer. After drying in air, the sample was examined by SEM (FEI Verios 460L) operating at 2 kV. For TEM characterization, the suspension was diluted with ethanol by a factor of 50 and cast onto a TEM lacey carbon grid (300 mesh) (Ted Pella). After drying in air, the sample was probed by TEM (JEOL 2010F and FEI Titan 80-300) operating at 200 kV.

Resistivity Measurement: Conductive paths were formed using a writing utensil (i.e., Sharpie) to press the top surface of the PDMS. The width of the indentation was measured using a digital Vernier caliper while the thickness of the conductive path was measured using optical microscope at the cross-section. A typical four-point probe measurement was set using a sourcemeter (Keithley 2400). Resistance was recorded after inserting tungsten (W) electrodes into the samples at different spots to vary the length of conductive traces.

Sintering Pressure Measurement: A PDMS microfluidic channel 50 mm long, 1 mm wide, and 50 μm high was fabricated using soft photolithography[39] from a commercial PDMS elastomer kit (Sylgard-184, Dow Corning). 100 nm thick "T shape" gold electrodes were deposited on glass slides (75 mm × 25 mm) using thermal deposition in order to achieve better electrical contact. Glass slides and PDMS microchannels were treated briefly with oxygen plasma and sealed together. The thickness of PDMS elastomer sheet varied from 0.5 to 3.7 mm. The 2 g/2 mL EGaIn/ethanol suspension was injected into the channels and dried in air. An extensometer (Instron 5943) was employed to perform the compression test (compression rate: 0.60 mm min^{-1}); the compression fixture was fabricated using 3D printing. Two gold electrodes were connected to a multimeter (Fluke 115) during the compression test. The critical pressure was recorded once the paths became conductive.

Morphology Study of the Microfluidic Devices: Microfluidic samples were fabricated using the procedure described in Figure 2. Some samples were mechanically sintered while some remained undisturbed. The bottom pads of PDMS elastomer were obtained by mechanically peeling the microfluidic devices apart. Those samples were probed by SEM (FEI Verios 460L) operating at 2 kV.

Supporting Information

Supporting Information is available from the Wiley Online Library or from the author.

Acknowledgements

The authors acknowledge funding from the National Science Foundation through CAREER (CMMI-0954321) and the Research Triangle MRSEC (DMR-1121107). The authors thank Dr. M. Rashed Khan for brainstorming on ideas pertaining to the fabrication of the antennas. The authors also acknowledge the use of the Analytical Instrumentation Facility (AIF) at North Carolina State University, which is supported by the State of North Carolina and the National Science Foundation. The authors also thank Dr. Yang Liu for TEM imaging. Y.L., J.G., and M.D.D. designed the project. Y.L., C.C., and M.W. performed the experiments. Y.L., J.G., and M.D.D. wrote the paper. All authors analyzed and interpreted the data. The authors declare no competing financial interests.

[1] J. A. Rogers, T. Someya, Y. Huang, *Science* **2010**, *327*, 1603.
[2] D.-H. Kim, J. Xiao, J. Song, Y. Huang, J. A. Rogers, *Adv. Mater.* **2010**, *22*, 2108.
[3] C. Keplinger, J.-Y. Sun, C. C. Foo, P. Rothemund, G. M. Whitesides, Z. Suo, *Science* **2013**, *341*, 984.
[4] D.-H. Kim, N. Lu, R. Ma, Y.-S. Kim, R.-H. Kim, S. Wang, J. Wu, S. M. Won, H. Tao, A. Islam, K. J. Yu, T. Kim, R. Chowdhury, M. Ying, L. Xu, M. Li, H.-J. Chung, H. Keum, M. McCormick, P. Liu, Y.-W. Zhang, F. G. Omenetto, Y. Huang, T. Coleman, J. A. Rogers, *Science* **2011**, *333*, 838.
[5] D.-Y. Khang, H. Jiang, Y. Huang, J. A. Rogers, *Science* **2006**, *311*, 208.
[6] H.-J. Koo, J.-H. So, M. D. Dickey, O. D. Velev, *Adv. Mater.* **2011**, *23*, 3559.
[7] T. Liu, P. Sen, C.-J. Kim, *J. Microelectromech. Syst.* **2012**, *21*, 443.
[8] M. D. Dickey, R. C. Chiechi, R. J. Larsen, E. A. Weiss, D. A. Weitz, G. M. Whitesides, *Adv. Funct. Mater.* **2008**, *18*, 1097.
[9] A. Russo, B. Y. Ahn, J. J. Adams, E. B. Duoss, J. T. Bernhard, J. A. Lewis, *Adv. Mater.* **2011**, *23*, 3426.
[10] S. Zhu, J.-H. So, R. Mays, S. Desai, W. R. Barnes, B. Pourdeyhimi, M. D. Dickey, *Adv. Funct. Mater.* **2013**, *23*, 2308.
[11] K. P. Mineart, Y. Lin, S. C. Desai, A. S. Krishnan, R. J. Spontak, M. D. Dickey, *Soft Matter* **2013**, *9*, 7695.
[12] S. J. French, D. J. Saunders, G. W. Ingle, *J. Phys. Chem.* **1938**, *42*, 265.
[13] J. N. Koster, *Cryst. Res. Technol.* **1999**, *34*, 1129.
[14] D. Zrnic, D. S. Swatik, *J. Common Met.* **1969**, *18*, 67.
[15] J.-H. So, J. Thelen, A. Qusba, G. J. Hayes, G. Lazzi, M. D. Dickey, *Adv. Funct. Mater.* **2009**, *19*, 3632.
[16] M. R. Khan, G. J. Hayes, J.-H. So, G. Lazzi, M. D. Dickey, *Appl. Phys. Lett.* **2011**, *99*, 013501.
[17] M. Kelley, C. Koo, H. McQuilken, B. Lawrence, S. Li, A. Han, G. Huff, *Electron. Lett.* **2013**, *49*, 1370.
[18] Y.-L. Park, C. Majidi, R. Kramer, P. Bérard, R. J. Wood, *J. Micromech. Microeng.* **2010**, *20*, 125029.

[19] R. K. Kramer, C. Majidi, R. Sahai, R. J. Wood, in *Intelligent Robots and Systems (IROS), 2011 IEEE/RSJ International Conference On* IEEE **2011**, p. 1919.
[20] A. Fassler, C. Majidi, *Smart Mater. Struct.* **2013**, *22*, 055023.
[21] E. Palleau, S. Reece, S. C. Desai, M. E. Smith, M. D. Dickey, *Adv. Mater.* **2013**, *25*, 1589.
[22] D. Tobjörk, H. Aarnio, P. Pulkkinen, R. Bollström, A. Määttänen, P. Ihalainen, T. Mäkelä, J. Peltonen, M. Toivakka, H. Tenhu, R. Österbacka, *Thin Solid Films* **2012**, *520*, 2949.
[23] M. Hösel, F. C. Krebs, *J. Mater. Chem.* **2012**, *22*, 15683.
[24] H.-S. Kim, S. R. Dhage, D.-E. Shim, H. T. Hahn, *Appl. Phys. A* **2009**, *97*, 791.
[25] J. Ryu, H.-S. Kim, H. T. Hahn, *J. Electron. Mater.* **2011**, *40*, 42.
[26] W.-H. Chung, H.-J. Hwang, S.-H. Lee, H.-S. Kim, *Nanotechnology* **2013**, *24*, 035202.
[27] S. H. Ko, H. Pan, C. P. Grigoropoulos, C. K. Luscombe, J. M. J. Fréchet, D. Poulikakos, *Nanotechnology* **2007**, *18*, 345202.
[28] J. W. Boley, E. L. White, R. K. Kramer, *Adv. Mater.* **2015**, *27*, 2355.
[29] A. Fassler, C. Majidi, *Adv. Mater.* **2015**, *27*, 1928.
[30] T. Yamada, Y. Hayamizu, Y. Yamamoto, Y. Yomogida, A. Izadi-Najafabadi, D. N. Futaba, K. Hata, *Nat. Nanotechnol.* **2011**, *6*, 296.
[31] Q. Cao, S.-H. Hur, Z.-T. Zhu, Y. G. Sun, C.-J. Wang, M. A. Meitl, M. Shim, J. A. Rogers, *Adv. Mater.* **2006**, *18*, 304.
[32] J. Lessing, S. A. Morin, C. Keplinger, A. S. Tayi, G. M. Whitesides, *Adv. Funct. Mater.* **2015**, *25*, 1418.
[33] J. Samson, A. Varotto, P. C. Nahirney, A. Toschi, I. Piscopo, C. M. Drain, *ACS Nano* **2009**, *3*, 339.
[34] J. Thelen, M. D. Dickey, T. Ward, *Lab Chip* **2012**, *12*, 3961.
[35] T. Hutter, W.-A. C. Bauer, S. R. Elliott, W. T. S. Huck, *Adv. Funct. Mater.* **2012**, *22*, 2624.
[36] J. N. Hohman, M. Kim, G. A. Wadsworth, H. R. Bednar, J. Jiang, M. A. LeThai, P. S. Weiss, *Nano Lett.* **2011**, *11*, 5104.
[37] R. C. Chiechi, E. A. Weiss, M. D. Dickey, G. M. Whitesides, *Angew. Chem.* **2008**, *120*, 148.
[38] R. L. Mays, M. D. Dickey, J. Genzer, *Lab Chip* **2013**, *13*, 4317.
[39] Y. Xia, G. M. Whitesides, *Angew. Chem. Int. Ed.* **1998**, *37*, 550.
[40] T. Shinsuke, Y. Hideki, T. Shoji, *J. Membr. Sci.* **1992**, *75*, 93.
[41] C. K. Yeom, S. H. Lee, H. Y. Song, J. M. Lee, *J. Membr. Sci.* **2002**, *198*, 129.

Received: September 4, 2015
Revised: September 30, 2015
Published online: November 16, 2015

